

## Time-Independent Finite Difference and Ghost Cell Method to Study Sloshing Liquid in 2D and 3D Tanks with Internal Structures

C. H. Wu<sup>1</sup>, O. M. Faltinsen<sup>2</sup> and B. F. Chen<sup>1,\*</sup>

<sup>1</sup> Department of Marine Environment and Engineering, National Sun Yat-Sen University, Kaohsiung 804, Taiwan.

<sup>2</sup> Centre for Ships and Ocean Structures & Department of Marine Technology, NTNU, Trondheim 7491, Norway.

Received 28 October 2011; Accepted (in revised version) 2 February 2012

Available online 29 August 2012

---

**Abstract.** A finite difference scheme with ghost cell technique is used to study viscous fluid sloshing in 2D and 3D tanks with internal structures. The Navier-Stokes equations in a moving coordinate system are derived and they are mapped onto a time-independent and stretched domain. The staggered grid is used and the revised SIMPLEC iteration algorithm is performed. The developed numerical model is rigorously validated by extensive comparisons with reported analytical, numerical and experimental results. The present numerical results were also validated through an experiment setup with a tank excited by an inclined horizontal excitation or a tank mounted by a vertical baffle. The method is then applied to a number of problems including sloshing fluid in a 2D tank with a bottom-mounted baffle and in a 3D tank with a vertical plate. The phenomena of diagonal sloshing waves affected by a vertical plate are investigated in detail in this work. The effects of internal structures on the resonant frequency of a tank with liquid are discussed and the present developed numerical method can successfully analyze the sloshing phenomenon in 2D or 3D tanks with internal structures.

**AMS subject classifications:** 65M06, 76B10, 49L25, 35Q35, 74F10

**Key words:** Liquid sloshing, baffle, plate, time-independent finite difference, ghost cell.

---

## 1 Introduction

Sloshing must be considered for almost any moving vehicle or structure containing a liquid with a free surface, such as tankers on highways, liquid oscillations in large storage tanks caused by earthquakes, sloshing of liquid cargo in ocean-going vessels and the

---

\*Corresponding author. *Email address:* chenbf@faculty.nsysu.edu.tw (B. F. Chen)

motion of liquid fuel in aircraft and spacecraft. Excitation with frequencies in the vicinity of the lowest natural frequency of the liquid motion is of primary practical interest. Resonant free-surface flows in tanks in aircraft, missiles and rockets have been the focus of extensive researches. The large amplitude of the liquid motion can create high impact pressures on the tank walls, which in turn can cause structural damage and may even create moments that affect the stability of the vehicle which carries the container. For these vehicles, sloshing will have a strong influence on their dynamic stability. The hydrodynamics of sloshing is complicated and the understanding of sloshing dynamics requires a combination of theory, computational fluid dynamics (CFD) and experiments.

The numerical, analytical and experimental studies of liquid sloshing in tanks have been reported in the past several decades and these studies have explored a range of significant phenomena such as the effect of fluid viscosity, linear and nonlinear effects and the classification of sloshing waves. If the interior of the tank is smooth, the fluid viscosity plays a minor role to affect the sloshing in tanks and an inviscid/irrotational potential flow solution is, therefore, suitable for describing the sloshing in a rigid tank. Abramson [1] provides a comprehensive review and discussion of early analytic and experimental studies of liquid sloshing, with application to the aerospace industry. In the recent studies, the series of studies by Faltinsen and his co-workers constitutes a major contribution to the field of sloshing. Faltinsen, Rognebakke and Timokha [2–4] extended their asymptotic modal system to model nonlinear sloshing in a 3D rectangular tank.

Besides the potential flow approaches, many numerical studies of the sloshing problem with primitive variables have been made, particularly when the fully nonlinear effects of the waves on the free surface are included. Papers that describe the modeling of two-dimensional or three-dimensional sloshing include Chen and Chiang [5], Sames, Marcouly and Schellin [6], Frandsen [7], Chen [8], Chen and Nokes [9], Akyildiz [10, 11] and more recent papers by Liu and Lin [12], Wu and Chen [13] and Chen and Wu [14]. The comprehensive discussions are reported by Faltinsen and Timokha [15].

Tuned liquid dampers (TLDs) are used to suppress horizontal vibrations of structures. A TLD consists of a tank partially filled with water. The lowest resonant frequency of sloshing is tuned to a structural natural frequency. Warnitchai and Pinkeaw [16] studied the mathematical model compared with experimental investigations for a rectangular tank with flow-damping devices. The vertical flat plate and the wire mesh screen can cause significant damping effects on sloshing waves. Isaacson and Premasiri [17] developed the mathematic solutions and experiment investigations to solve the hydrodynamic damping due to baffles in a fluid-filled rectangular tank undergoing horizontal motions. The average rate of energy dissipation due to flow separation around baffles and the total energy of sloshing waves were used to estimate the hydrodynamic damping.

Biswal et al. [18] used FEM (Finite element method) on computing the non-linear sloshing response of liquid in a two-dimensional rectangular tank and a circular cylindrical container with rigid baffles. The effect of baffle parameters including length, numbers and position on sloshing response were discussed. A 3D FEM model for liquid sloshing in a baffled tank was adopted by Firouz-Abadi et al. [19]. The determinations of the nat-

ural frequencies and mode shapes of liquid sloshing in 3D baffled tanks with arbitrary geometries were investigated. However, the potential flow assumption used in FEM cannot predict the effect of energy dissipation due to viscous sloshing and flow separation. Kim [20] and Kim et al. [21] employed the SLOA (solution algorithm) scheme to study the 3D liquid sloshing with baffles in tanks and compared the impact pressure with that of an unbaffled tank. Liu and Lin [22] used NEWTANK (Numerical Wave Tank) to investigate liquid sloshing in a 3D baffled tank with LES (Large-eddy-simulation). In their study, the vertical baffle is a more effective tool in reducing the sloshing amplitude in tanks. Panigrahy et al. [23] did a series of experiment of liquid sloshing in a tank with and without different types of baffles under various fill depths. They concluded that the introduction of baffles in the tank decreases effectively the sloshing displacement because the sharp-edged baffles could dissipate the kinetic energy by generating turbulence in the flow and a type of ring baffles are the most effective device to reduce sloshing energy.

In this work, experiments of a 3D tank oscillated at various excitation angles was set up and the results were used to validate the present numerical simulation obtained by the proposed finite difference method. The experiment was further extended to investigate liquid motions in a tank with a vertically tank bottom-mounted baffle. The comparison of the results between the experimental measurements and the present computations shows an excellent agreement. The present numerical model is then applied on the analysis of liquid sloshing in the tank with internal structures, such as baffles. The treatment of flow field around baffles is carried out by one dimensional ghost cell approach [24] and the second order upwind scheme [25]. The phenomena of vortex generation and flow separation due to baffles are presented as well. The influence of baffles inside the tank on the natural frequencies of the tank is discussed in detail. Section 2 introduces the equations of motion which are written in a moving coordinate system. The proposed finite-difference method is introduced in Section 3. Besides, the one-dimensional ghost cell approach [24] is implemented to deal with the fluid-structure domain, especially for the structures with the sharp corners. The comprehensive benchmark tests of the present numerical scheme are demonstrated in Section 4 and the setup of the experiment is included as well. The investigations of tuned liquid damper (TLD) for 2D and 3D tanks are also dissected in the section. Section 5 summarizes the key conclusions.

## 2 Mathematical formulations

In this work, a rigid tank partially filled with fluid is considered and analyzed by a time-independent finite difference method [9] to simulate the movement of sloshing waves in a tank with and without internal structures. As illustrated in Fig. 1, the breadth of tank is  $L$ , the tank's width is  $B$  and  $d_0$  is the still water depth. The Navier-Stokes equations written in a moving coordinate system can be expressed as

$$\frac{\partial u}{\partial t} + u \frac{\partial u}{\partial x} + v \frac{\partial u}{\partial y} + w \frac{\partial u}{\partial z} = -\frac{1}{\rho} \frac{\partial p}{\partial x} - x_C + \nu \left( \frac{\partial^2 u}{\partial x^2} + \frac{\partial^2 u}{\partial y^2} + \frac{\partial^2 u}{\partial z^2} \right), \quad (2.1a)$$

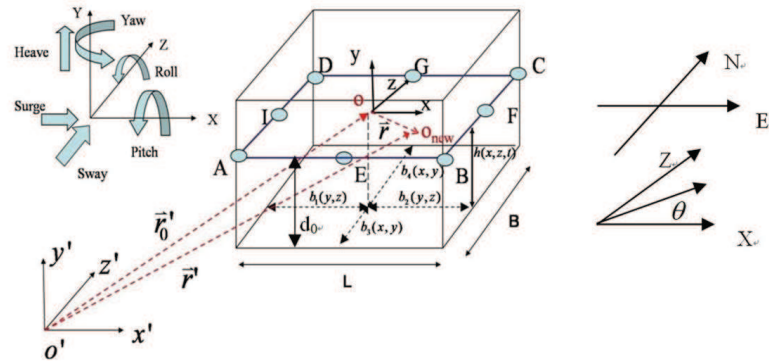


Figure 1: Definition sketches of the tank and the coordinate system.

$$\frac{\partial v}{\partial t} + u \frac{\partial v}{\partial x} + v \frac{\partial v}{\partial y} + w \frac{\partial v}{\partial z} = -g - \frac{1}{\rho} \frac{\partial p}{\partial y} - y_c + \nu \left( \frac{\partial^2 v}{\partial x^2} + \frac{\partial^2 v}{\partial y^2} + \frac{\partial^2 v}{\partial z^2} \right), \quad (2.1b)$$

$$\frac{\partial w}{\partial t} + u \frac{\partial w}{\partial x} + v \frac{\partial w}{\partial y} + w \frac{\partial w}{\partial z} = -\frac{1}{\rho} \frac{\partial p}{\partial z} - z_c + \nu \left( \frac{\partial^2 w}{\partial x^2} + \frac{\partial^2 w}{\partial y^2} + \frac{\partial^2 w}{\partial z^2} \right), \quad (2.1c)$$

where  $u, v$  and  $w$  are the relative velocity components in the respective  $x, y$  and  $z$  directions,  $x_c, y_c$  and  $z_c$  are the relative acceleration components of the tank in the respective  $x, y$  and  $z$  directions;  $p$  is the pressure,  $\rho$  is the fluid density,  $\nu$  is kinematic viscosity of the fluid and  $g$  is the acceleration due to gravity.

The continuity equation for incompressible flow is

$$\frac{\partial u}{\partial x} + \frac{\partial v}{\partial y} + \frac{\partial w}{\partial z} = 0. \quad (2.2)$$

The kinematic condition states that the fluid particles at a free surface remain on the free surface, and it can be expressed as

$$\frac{\partial \eta}{\partial t} + u \frac{\partial \eta}{\partial x} + w \frac{\partial \eta}{\partial z} = v. \quad (2.3)$$

Where  $\eta(x, z, t) = h(x, z, t) - d_0$  is the elevation of free surface measured from the undisturbed water depth  $d_0$ . The dynamic condition requires that the normal stress is equal to the atmospheric pressure and the two tangential stresses are zero along the free surface boundary. The dynamic conditions can be expressed as follows:

$$P_F = \frac{y}{Fr^2} + \frac{2[u_x \eta_x^2 + w_z \eta_z^2 + v_y + (u_z + w_x) \eta_x \eta_z - (u_y + v_x) \eta_x - (v_z + w_y) \eta_z]}{Re(\eta_x^2 + \eta_z^2 + 1)}, \quad (2.4a)$$

$$u_y = -v_x + \frac{2(u_x - v_y) \eta_x + (u_z + w_x) \eta_z + (v_z + w_y) \eta_x \eta_z}{1 - \eta_x^2}, \quad (2.4b)$$

$$w_y = -v_z + \frac{2(w_z - v_y) \eta_z + (u_z + w_x) \eta_x + (v_z + u_y) \eta_x \eta_z}{1 - \eta_z^2}, \quad (2.4c)$$

where  $Fr$  is the Froude number and  $Re$  is the Reynolds number that are defined as

$$Fr = \frac{u_m}{\sqrt{gd_0}}, \quad Re = \frac{u_m d_0}{\nu}, \quad (2.5)$$

where  $u_m = \omega a_0$  ( $\omega$  is the angular velocity and  $a_0$  is the excitation displacement of the tank) is the maximum velocity of the tank. And  $\eta_x$  denotes a partial derivative of  $\eta$  with respect to  $x$  and others have the same meanings. In the present study, Eq. (2.4a) is used to determine the hydrodynamic pressure at the free surface, while Eqs. (2.4b) and (2.4c) are used to extrapolate the horizontal velocity ( $u, w$ ) at the free surface from the flow domain.

Taking partial derivatives of Eqs. (2.1a), (2.1b) and (2.1c) with respect to  $x$ ,  $y$  and  $z$  respectively and summing the results, one can obtain the following equation to solve for the pressure

$$\begin{aligned} \frac{\partial^2 p}{\partial x^2} + \frac{\partial^2 p}{\partial y^2} + \frac{\partial^2 p}{\partial z^2} = & -\rho \frac{\partial}{\partial x} \left( u \frac{\partial u}{\partial x} + v \frac{\partial u}{\partial y} + w \frac{\partial u}{\partial z} \right) - \rho \frac{\partial}{\partial y} \left( u \frac{\partial v}{\partial x} + v \frac{\partial v}{\partial y} + w \frac{\partial v}{\partial z} \right) \\ & - \rho \frac{\partial}{\partial z} \left( u \frac{\partial w}{\partial x} + v \frac{\partial w}{\partial y} + w \frac{\partial w}{\partial z} \right). \end{aligned} \quad (2.6)$$

## 2.1 The coordinate transformation

Many finite difference and finite volume methods have been reported to solve the free surface displacement of sloshing fluid in tanks. Among these methods, MAC (Marker and Cell), VOF (Volume of Fluid) and LS (Level set) are the most well-known. A brief review of these methods can be referred to [9]. In contrast, the present study uses simple mapping functions to remove the time-dependence of the free surface of the fluid domain. The irregular boundaries, including the time-varying fluid surface, non-vertical walls and non-horizontal bottom, can be mapped onto a cube by the proper coordinate transformations [9, 26, 27] and those descriptions are omitted here.

The convenience of the coordinate transformations is to map a wavy and time-dependent fluid domain onto a time-independent unit cubic domain for computing. It will, however, encounter some problems by implementing the coordinate transformations while the internal structures, for example, baffles or plates, are mounted inside the tank. The problems mainly occur among the domain that the violent interaction between the fluid and the internal structures, especially for irregular sharp geometries. As illustrated in Fig. 2, a structure with sharp corners surrounded with regular grids but the connection between the structure boundary and grids is abnormal due to the deformation of the free surface with time. In the present study, it is hard to solve the boundary condition of the structure surrounded by irregular meshes by using the finite different method. The further coordinate transformation, therefore, is developed. Let's take a 2D tank with a vertically bottom-mounted baffle (see Fig. 3) as an example. As listed in Fig. 3, the distance from the tank west wall to the baffle center is  $X_b$  and the distance between the free surface and the baffle tip is  $Y_b$ . We divide the fluid domain into two parts in the  $x$

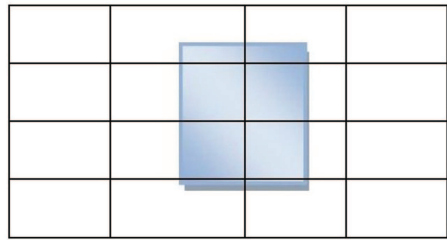


Figure 2: A structure with sharp corners immerses in the regular grid system.

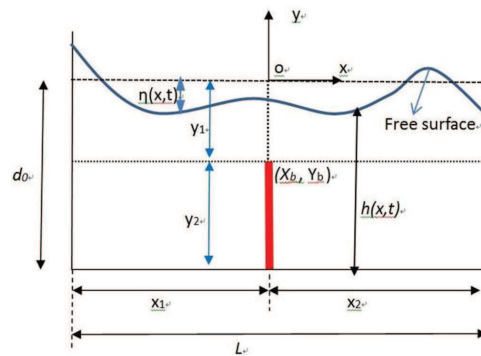


Figure 3: The new coordinate transformation on the tank with a tank bottom-mounted baffle.

and  $y$  axes based on the location and the height of the baffle. The new mapping functions of coordinate transformation can be expressed as

$$x_1^* = \frac{x_1}{X_b} \qquad x_2^* = \frac{x_2}{L - X_b} \qquad (2.7a)$$

$$y_1^* = 1 - \frac{y_1 + d_0 - Y_b}{h(x,z,t) - Y_b} \qquad y_2^* = -\frac{y_2}{Y_b}. \qquad (2.7b)$$

Through the mapping functions in Eq. (2.7), one can map the west wall to  $x_1^* = 0$  and the baffle center to  $x_1^* = 1$  and  $x_2^* = 0$  and the east wall to  $x_2^* = 1$ ; the free surface to  $y_1^* = 0$  and the baffle tip to  $y_1^* = 1$  and  $y_2^* = 0$  and the tank bottom to  $y_2^* = 1$ . In this way, the transformations can be used not only to apply on the tank with internal structures at various positions and heights but to avoid the internal structures surrounded by irregular meshes. Further, the stretching technique [13] is also adopted in this work and the stretching grids can be arranged around the structure with sharp corners. For a 3D tank, the new function of coordinate transformation in the  $z$  axis is

$$z_1^* = \frac{z_1}{Z_b} \qquad z_2^* = \frac{z_2}{B - Z_b}, \qquad (2.8)$$

where  $Z_b$  is the distance from the south wall to the baffle center in the  $z$  axis.

## 2.2 Dimensionless equations

All the numerical results presented in this work are in the dimensionless form listed as follows. The dimensional parameters are normalized [14] and the momentum equation (as an example) in the  $x$ -direction can, then, be expressed as

$$\begin{aligned}
 & U_T + (C_{10}C_{13}U_X + C_{11}C_{14}U_Y + C_{12}C_{15}U_Z) + C_1C_{13}UU_X + C_2C_{14}UU_Y + C_3C_{15}UU_Z \\
 & + C_4C_{13}VU_X + C_5C_{14}VU_Y + C_6C_{15}VU_Z + C_7C_{13}WU_X + C_8C_{14}WU_Y + C_9C_{15}WU_Z \\
 & = -\frac{g_x}{g} - (C_1C_{13}P_X + C_2C_{14}P_Y + C_3C_{15}P_Z) - \ddot{X}_C + \frac{1}{Re} \left( C_1C_{13} \frac{\partial R_{1x}}{\partial X} + C_2C_{14} \frac{\partial R_{1y}}{\partial Y} \right. \\
 & + C_3C_{15} \frac{\partial R_{1z}}{\partial Z} + C_4C_{13} \frac{\partial R_{2x}}{\partial X} + C_5C_{14} \frac{\partial R_{2y}}{\partial Y} + C_6C_{15} \frac{\partial R_{2z}}{\partial Z} + C_7C_{13} \frac{\partial R_{3x}}{\partial X} \\
 & \left. + C_8C_{14} \frac{\partial R_{3y}}{\partial Y} + C_9C_{15} \frac{\partial R_{3z}}{\partial Z} \right), \tag{2.9a}
 \end{aligned}$$

$$R_{1x} = C_1C_{13} \frac{\partial U}{\partial X} + C_2C_{14} \frac{\partial U}{\partial Y} + C_3C_{15} \frac{\partial U}{\partial Z}, \quad R_{1y} = C_1C_{13} \frac{\partial U}{\partial X} + C_2C_{14} \frac{\partial U}{\partial Y} + C_3C_{15} \frac{\partial U}{\partial Z}, \tag{2.9b}$$

$$R_{1z} = C_1C_{13} \frac{\partial U}{\partial X} + C_2C_{14} \frac{\partial U}{\partial Y} + C_3C_{15} \frac{\partial U}{\partial Z}, \quad R_{2x} = C_4C_{13} \frac{\partial U}{\partial X} + C_5C_{14} \frac{\partial U}{\partial Y} + C_6C_{15} \frac{\partial U}{\partial Z}, \tag{2.9c}$$

$$R_{2y} = C_4C_{13} \frac{\partial U}{\partial X} + C_5C_{14} \frac{\partial U}{\partial Y} + C_6C_{15} \frac{\partial U}{\partial Z}, \quad R_{2z} = C_4C_{13} \frac{\partial U}{\partial X} + C_5C_{14} \frac{\partial U}{\partial Y} + C_6C_{15} \frac{\partial U}{\partial Z}, \tag{2.9d}$$

$$R_{3x} = C_7C_{13} \frac{\partial U}{\partial X} + C_8C_{14} \frac{\partial U}{\partial Y} + C_9C_{15} \frac{\partial U}{\partial Z}, \quad R_{3y} = C_7C_{13} \frac{\partial U}{\partial X} + C_8C_{14} \frac{\partial U}{\partial Y} + C_9C_{15} \frac{\partial U}{\partial Z}, \tag{2.9e}$$

$$R_{3z} = C_7C_{13} \frac{\partial U}{\partial X} + C_8C_{14} \frac{\partial U}{\partial Y} + C_9C_{15} \frac{\partial U}{\partial Z}. \tag{2.9f}$$

The definition of  $R_{ij}$  ( $i = 1, 2, 3, j = 1, 2, 3$ ) and the dimensionless forms of the other governing equations are omitted in the text. In Eq. (2.9),  $C_1$ - $C_{15}$  are the coefficients that arise from the coordinate transformations and can be referred to Chen and Wu [14].  $P_X$  denotes a partial derivative of  $P$  with respect to  $X$  and  $U_T$  is the partial derivative of  $U$  with respect to dimensionless time  $T$ . All other terms have similar meanings. For a fully nonlinear free surface condition, the kinematic free surface condition must be applied at the instantaneous free surface location, i.e., at  $\eta = h(x, z, t) - d_0$ . Thus, the coefficients  $C_1$ - $C_{15}$  related to the free surface position are updated during iterations.

## 3 Computational algorithm

In this three-dimensional analysis, the fluid flow is solved in a unit cubic mesh in the transformed flow domain. Central difference approximations are used for the space derivatives and the forward or backward difference is employed at the boundary. A staggered grid system is used in the analysis. The detailed finite difference scheme and the revised SIMPLEC iterative procedure are omitted in the text and they can be referred to [14]. Besides, the second-order central difference and first order upwind scheme [25]

are implemented in this work. The present numerical scheme has been parallelized by using MPI (Message passing interface), particularly when liquid sloshing in a 3D tank with internal structures is considered. The efficiency of the present numerical approach can be referred to [13,14], where the grid numbers and the time step used in this work were compared to the reported simulation by Kim [20]. The present computation can get an accurate result with a less grid number and a larger time step. The accuracy of the numerical results significantly depends on the spatial grid resolution and the selected time step. The numerical errors can be reduced if the time step is restricted by the condition given in Eq. (3.1)

$$\Delta t < \min \left\{ \frac{\Delta x_{\min}}{|u_{i,j,k}|}, \frac{\Delta y_{\min}}{|v_{i,j,k}|}, \frac{\Delta z_{\min}}{|w_{i,j,k}|} \right\}, \quad v\Delta t < \frac{1}{2} \frac{\Delta x_{\min}^2 \Delta y_{\min}^2 \Delta z_{\min}^2}{\Delta x_{\min}^2 + \Delta y_{\min}^2 + \Delta z_{\min}^2}. \quad (3.1)$$

The first term in Eq. (3.1) implies that a fluid particle cannot move more than one cell in a single time step. The second ensures that the diffusion of momentum is not significant over more than one cell in one time step.

### 3.1 A one-dimensional ghost cell approach

Traditional finite difference methods cannot work well on the discontinuous and non-smooth functions since the Taylor expansion is not valid for such problems. As illustrated in Fig. 4, a structure with sharp corners immersed into the fluid. It is tricky to apply the finite difference methods on the discontinuous fluid-structure domain and the grids with filled color need to be carefully treated. But, if the function is piecewise smooth, it is possible to devise a technique that conforms to any jump in the function and its higher derivatives. It would cause some problems that the finite difference approximations of the convective terms are expressed on the filled color areas, especially for  $u\partial u/\partial y$  and  $v\partial v/\partial x$ . If the forward or the backward finite difference representation of  $u\partial u/\partial y$  or  $v\partial v/\partial x$  is implemented, the influence of the sharp corner *A* or *B* on the vicinity of the fluid could be neglected. By doing this, however, the interaction between the fluid and the structure is not considered which might result in incorrect results due to neglecting the effect of the sharp corners. The function of implementing the one-dimensional ghost cell approach is to continue the fluid domain inside the structure by utilizing the polynomial approximation. The general central difference approximation of  $u\partial u/\partial y$  and  $v\partial v/\partial x$  are expressed as

$$u \frac{\partial u}{\partial y} = u \frac{u_{i,j+1} - u_{i,j-1}}{\Delta y}, \quad v \frac{\partial v}{\partial x} = v \frac{v_{i+1,j} - v_{i-1,j}}{\Delta x}. \quad (3.2)$$

As depicted in Fig. 4(b), the positions of  $u_{i,j-1}$  and  $v_{i,j-1}$  are on the structure boundary and their values are assumed zero in general. This also makes some problems because of ignoring the effect of the sharp corners. We, therefore, replace the positions of  $u_{i,j-1}$  and  $v_{i,j-1}$  with the ghost points  $U_g$  and  $V_g$  and the values of  $U_g$  and  $V_g$  are given by the

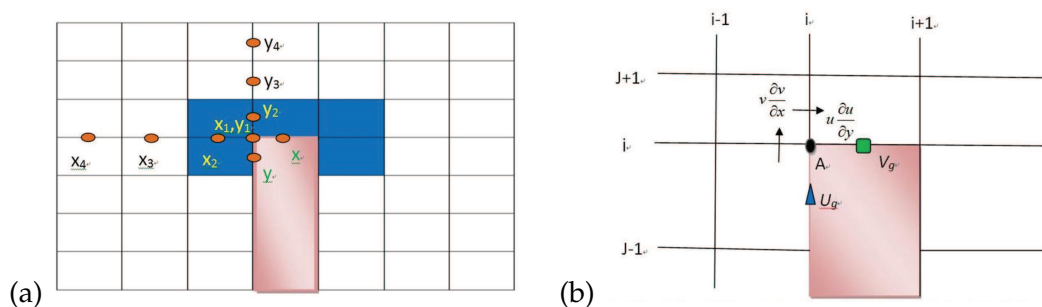


Figure 4: Illustration of the ghost cells and the polynomial extrapolation around the sharp corner  $A$ .

extrapolating polynomial of three degree through 4 points that are expressed as

$$U_g = \sum_{j=1}^4 U_j \prod_{i=1}^4 \frac{y-y_i}{y_j-y_i}, \quad V_g = \sum_{j=1}^4 V_j \prod_{i=1}^4 \frac{x-x_i}{x_j-x_i}, \quad (3.3)$$

where  $x$  and  $y$  are the coordinates of  $V_g$  and  $U_g$ , respectively and the locations of  $x_1 \sim x_4$  and  $y_1 \sim y_4$  are marked in Fig. 4(a) that represent the coordinate of  $V_1 \sim V_4$  and  $U_1 \sim U_4$ , respectively. It is noted that the values of  $U_1$  and  $V_1$  are set to be 0 because of the no-slip boundary condition on the corner  $A$ . Through the polynomial extrapolation, the fluid domain could be assumed continually penetrating the structure. As the free surface deforms with time, so does the coordinate system in the  $y$  axis. As a result, the polynomial extrapolations of  $U_g$  and  $V_g$  have to be updated instantaneously at each time step. Further, the treatment of diffusion terms of momentum equations near the structure boundaries also can be implemented by the method described above.

## 4 Results and discussion

At first, the validation of the present numerical scheme is definitely of importance and, therefore, a series of benchmark tests compared with the reported experimental, analytical and numerical solutions have been rigorously done in the present work. The convergence (stability) study of numerical results is also illustrated. The experiment of a 3D tank with or without internal structures under coupled surge-sway motion is instituted as well to carry out further investigation of liquid sloshing.

### 4.1 Stability analysis and the benchmark tests

In this section, a tank without internal structures is considered to demonstrate the accuracy of the developed time-independent finite difference method applied on liquid sloshing.

#### 4.1.1 Convergence study

The accuracy of numerical results significantly depends on the numbers of grid and the time step chosen for each problem. Accordingly, the proper grid system and time step are needed to be verified before large numerical cases to be simulated. We consider a rectangular tank with breadth/width =  $L/B=1$ , still water depth/breadth =  $d_0/L=0.25$ , the ground accelerations of surge, heave and sway motions are given as

$$x_c = x_0 \omega_x^2 \sin \omega_x t, \quad y_c = y_0 \omega_y^2 \sin \omega_y t, \quad z_c = z_0 \omega_z^2 \sin \omega_z t, \quad (4.1)$$

where  $x_0$ ,  $y_0$  and  $z_0$  are the excited amplitudes of the tank and  $\omega_x$ ,  $\omega_y$  and  $\omega_z$  are the corresponding excited frequency with respect to surge, heave, and sway motions; For the convergence study, we assume the tank's motion is oscillated in the diagonal direction ( $\theta = 45^\circ$ ) with an excitation frequency of  $0.9\omega_l$  ( $\omega_l$ : the lowest natural frequency of the tank) and the ratio of the excitation displacement/tank breadth =  $a_0/L = 0.005$  that implies  $x_0 = a_0 \cos \theta$  and  $z_0 = a_0 \sin \theta$ .

Fig. 5(a) presents the effect of the variation of grid numbers with a fixed dimensionless time step  $\Delta T = 0.00626$  ( $T = t\sqrt{g/d_0}$ ) on the simulation and the results shown in the figure indicate the influence of various grid numbers on the computational result is insignificant. The effect of the varied time steps with a fixed grid number ( $20 \times 10 \times 20$ ) depicted in Fig. 5(b) shows the computational results of different cases are almost the same with the decrease of time step. This means the present numerical results obtain an excellent convergence in the grid numbers ( $20 \times 10 \times 20$ ) and the time step = 0.00626. The parametric study of the stretching constants was also done [19] and the stretching constants  $\lambda_1 = \lambda_2 = \lambda_3$ ,  $k_1 = k_2 = k_3 = 2$  are used in this study.

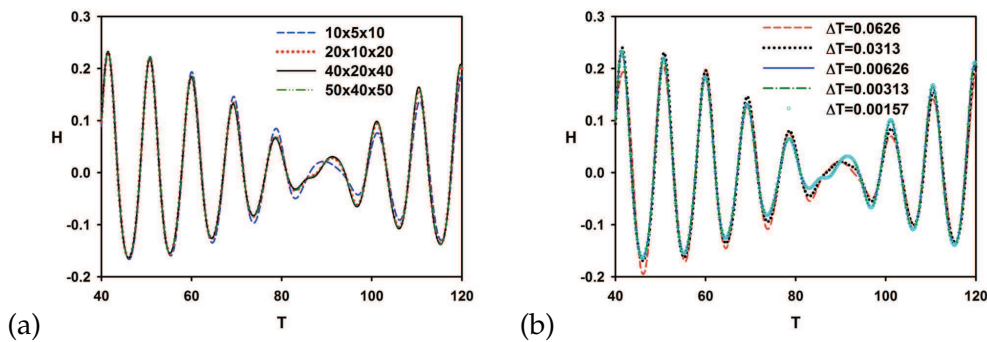


Figure 5: The convergence study of the wave history at corner  $A$  for a tank under diagonal excitation. The influence of (a) grid numbers; (b) time step.  $H = \eta/d_0$  is the dimensionless wave elevation,  $T = t\sqrt{g/d_0}$  is the dimensionless time.  $B/L=1$ ,  $d_0/L=0.25$ ,  $a_0/L=0.005$ ,  $\omega_x = \omega_z = 0.9\omega_l$ ,  $\theta = 45^\circ$ .

#### 4.1.2 Benchmark tests

In order to further validate the accuracy of our model, we compare our results to those reported in the literature. Fig. 6 presents the comparison between the present numerical

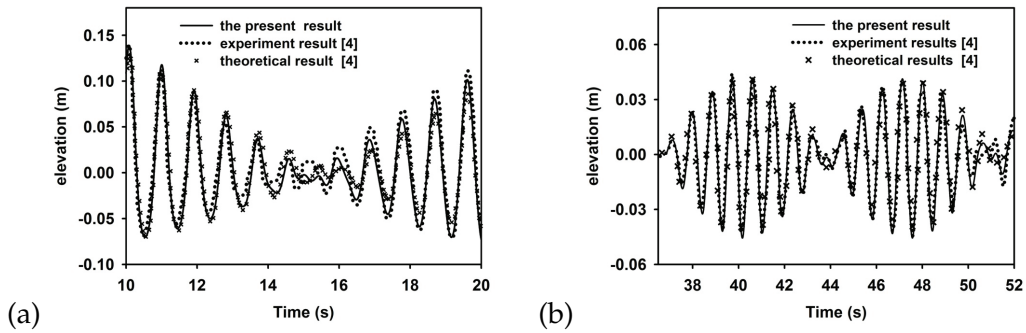


Figure 6: The comparisons between experimental measurement, analytical results, and the present results of wave elevation (near point  $F$ ),  $d_0/L=0.5$ ,  $a_0/L=0.005$ . (a) Surge motion,  $\omega_x=1.037\omega_1$ ; (b) diagonal motion,  $\omega_x=\omega_z=1.115\omega_1$ .

result and the experimental and theoretical results reported by Faltinsen et al. [4] as the tank excited in only surge or diagonal motion and the agreements are very good.

### 4.1.3 Experiment investigation

Information on the experimental investigation of sloshing in published literature is very limited and the major work done by Faltinsen et al. [2–4,28] only concentrated on a tank excited at only the longitudinal ( $\theta=0^\circ$ ) or diagonal ( $\theta=45^\circ$ ) direction. In reality, as the tank is excited by accelerations due to an earthquake or waves, the excitation directions include multi-degrees of freedom (surge/sway/heave/pitch/roll/yaw) and the excitation frequency also varies with time. In view of this, an experiment program was conceived in an attempt to carry out some preliminary investigation on the effect of sloshing in tanks oscillated with various excitation angles and to further validate the accuracy of the present numerical work.

An experiment setup is illustrated in Fig. 7(a), and the tank attached to a shaking table which can be moved back and forth with various excitation angles by an AC motor.

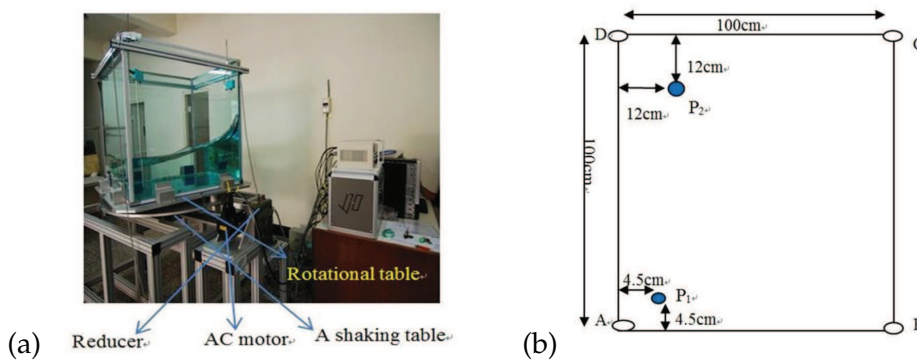


Figure 7: (a) The experiment setup; (b) positions of the wave probes.

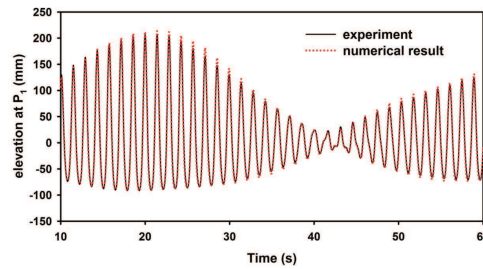


Figure 8: The comparison between the results of experimental measurement at probe  $P_1$  and numerical simulation.  $B/L=1$ ,  $d_0/L=0.25$ ,  $a_0/L=0.005$ ,  $\omega_x=\omega_z=0.97\omega_1$ ,  $\theta=15^\circ$ .

The excitation direction of the shaking table is designed to be altered by an aluminum alloy rotational table. The maximum moving distance ( $r$ ) of the shaking table is 30mm and the highest revolutions of the motor is 2000r.p.m. The frequency level depends on the limitation of the maximum velocity implemented by the AC motor and the motor reducer. In this experiment of work, the maximum velocity ( $V_m=\omega_r$ ) of the shaking table is about 30mm/s that indicates if the excitation displacement ( $r$ ) becomes large, the corresponding excitation frequency has to be reduced. The material of the tank is made by tempered glass with 20mm thickness to prevent the tank deformation from the impact of the hydrostatic and hydrodynamic pressure of the fluid. The measurement of wave elevation is carried out by wave probes and the locations of wave probes,  $P_1$  and  $P_2$ , are depicted in Fig. 7(b). A near-resonant case is initially implemented that the excitation frequency of the fluid-filled tank is  $0.97\omega_1$  with an excitation angle of  $15^\circ$ . The excitation amplitude is 5mm which is under the tolerance of the present experimental device. After a great number of experimental tests have been performed, the experimental data are filtered and then averaged by picking up 15 cases of measured data with minor differences. Fig. 8 presents the comparison between the results of experimental measurement and numerical simulation and a good agreement is shown. The wave troughs of experimental result correspond exactly with that of numerical simulation and the wave peaks,

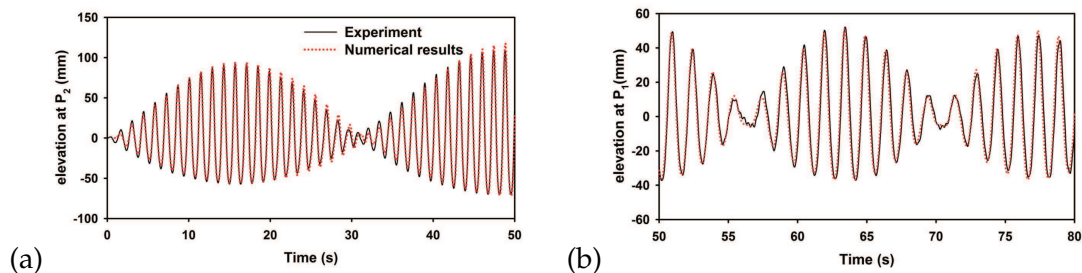


Figure 9: The comparison between the present results of experiment and numerical simulation under various excitation angles and excitation frequencies.  $B/L=1$ ,  $d_0/L=0.25$ ,  $a_0/L=0.005$ . (a) The measured data of wave elevation at wave probe  $P_2$ ,  $\omega_x=\omega_z=0.97\omega_1$ ,  $\theta=5^\circ$ ; (b) the measured data of wave elevation at wave probe  $P_1$ ,  $\omega_x=\omega_z=0.90\omega_1$ ,  $\theta=30^\circ$ .

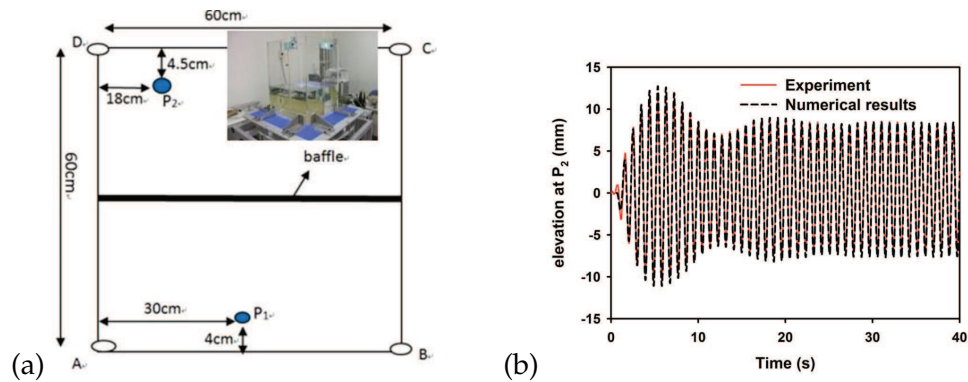


Figure 10: (a) Positions of the wave probes from the top view of the baffled tank; (b) The comparison between the results of experiment and the present numerical simulation,  $d_0/L=0.5$ ,  $d_b/d_0=0.5$ ,  $a_0/L=0.002$ ,  $\omega_x=1.0\omega_1$ ,  $\theta=0^\circ$ .

however, display a little difference between them. With various excitation angles and excitation frequencies, the more experimental measurements compared with the present numerical results are depicted in Fig. 9 and the excellent agreement is presented as well. As a result, the present numerical model is an efficient and accurate tool to simulate the dynamic response of liquid sloshing in 3D tanks.

The experiment of liquid sloshing in a tank with a vertically tank bottom-mounted baffle is also considered in this work. Fig. 10(a) presents the photography of the experiment (see the subplot) and the locations of the wave probes. The comparison of the wave elevation at probe  $P_2$  between the experimental measurement and the numerical calculation for a baffled tank under surge motion is illustrated in Fig. 10(b) and an excellent agreement is demonstrated. Accordingly, the present numerical scheme can be applied on the study of liquid dynamics in tanks with internal structures.

#### 4.2 A tank with internal structures (Tuned liquid damper)

A Tuned Liquid Damper (TLD) is one possible damping device uses in tall buildings under wind and earthquake excitations. Ship motions excite sloshing, which in return affects the ship's motions. Ships equipped with anti-rolling tanks utilize this effect. The sloshing-induced roll moment on the vessel will cause roll damping if the lowest natural sloshing period is tuned to be close to the roll natural period. For the study made by Faltinsen & Timokha [15], the asymptotic formula shows that if vertical baffles are mounted to the bottom of a rectangular tank and the liquid depth is finite, their effect on the natural mode is, in general, negligible as long as the distance between their edges and the mean free surface is larger than  $0.2L$  ( $L$ : the horizontal dimension of the tank). When the liquid depth becomes smaller or the distance decreases, the effect of the baffle on the natural sloshing modes and frequencies becomes important. In this study, a vertically tank bottom-mounted baffle or a vertical plate in a partially fluid-filled tank are considered.

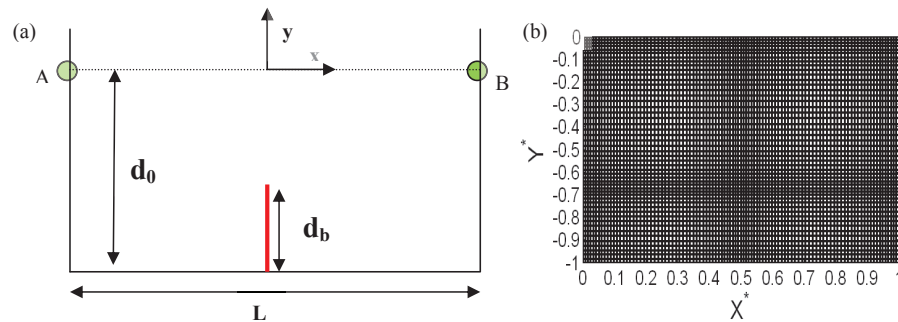


Figure 11: (a) Definition sketch and (b) stretching grids for a vertically tank bottom-mounted baffle at the middle point of the tank.  $d_b = 0.3d_0$ .

#### 4.2.1 A vertical baffle mounted at the middle of tank bottom

The vertically bottom-mounted baffle on a rectangular tank is depicted in Fig. 11, where  $d_b$  is the height of the baffle. The stretching meshes are implemented and focus on the tip of the baffle, as shown in Fig. 11(b). The comparison between the present result and the reported numerical result [22] is shown in Fig. 12 and the results present a good agreement. The further comparison of velocity vectors at  $t = 5.05$  seconds is displayed in Fig. 13(a). The vortex shedding generated near the left and right sharp corners of the baffle can be obviously seen in the present results. However, this phenomenon didn't appear in Liu's study [22]. In other words, the stretch technique of grid system [13] implemented in the present study assures the finer meshes around the tip of the baffles and the numerical simulation in this work can, therefore, capture the detailed local phenomenon of flow movement around the tip. For a longer time simulation, the effect of vortex shedding on the flow domain cannot be neglected in terms of the energy dissipation and the development of turbulent flow. As conspicuously depicted in Fig. 13(b), the movement of vortices towards the free surface resulted in the energy dissipation of sloshing waves.

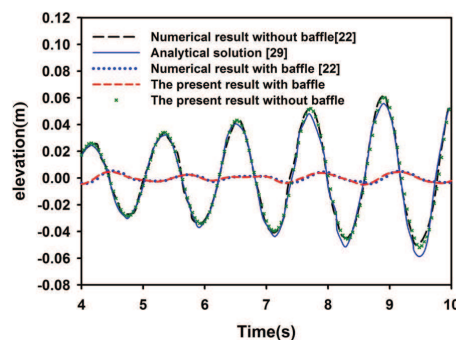


Figure 12: The comparison of the wave elevation at point B between the present results and the numerical results [22] and the analytic solution [29]. A tank excited in surge motion with or without a vertically tank bottom-mounted baffle.  $d_0/L = 0.5$ ,  $d_b/d_0 = 0.75$ ,  $x_0 = 0.002L$ ,  $\omega_x = 1.0\omega_1$ .

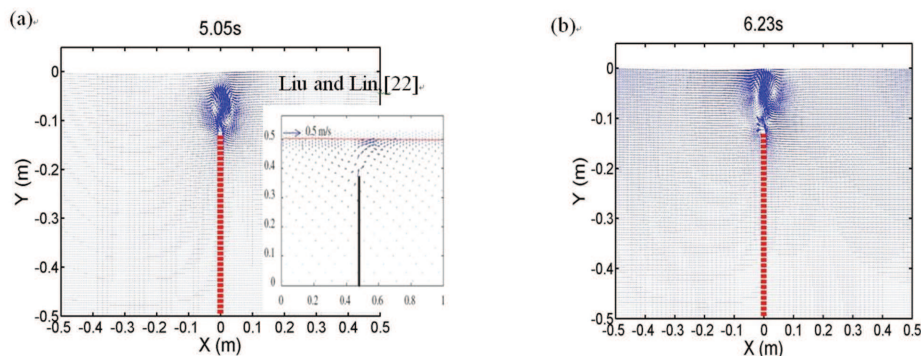


Figure 13: The phenomenon of vortex shedding. The same as in Fig. 12.

The influence of a vertically tank bottom-mounted baffle inside a tank on the natural frequency of the container is, then, presented. The comparison between the present result, the asymptotic formula [15] and the numerical result reported by Firoua-Abadi [19], as depicted in Fig. 14, agree well when  $d_b/d_0 \leq 0.3$ . For larger ratio of  $d_b/d_0$ , the asymptotic formula [15] is inadequate to predict the influence of internal baffles on the natural frequency of the tank. Based on the assumption of potential flow, the boundary element method [19] cannot describe the phenomenon of flow separation that would cause energy dissipation to affect the natural frequency of liquid sloshing in tanks. As  $d_b/d_0$  is close to 1, which means the baffle is beneath the free surface for a small distance, the obvious influence of the baffle on the natural frequency of the tank is significant.

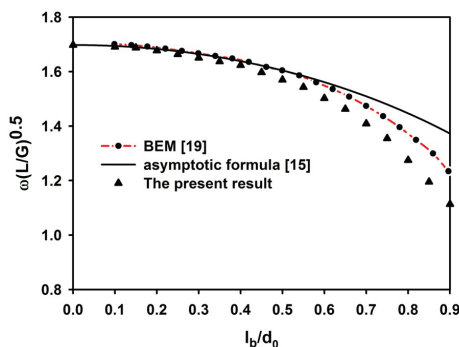


Figure 14: The non-dimensional frequency versus baffle height-to-liquid depth  $d_b/d_0$  for a vertically tank bottom-mounted baffle at the middle point with the liquid depth-to-tank height  $d_0/L=0.5$ .

### 4.2.2 A 3D tank with a vertical plate

In this section, a 3D tank with a vertical plate mounted in the middle of the tank is presented and the definition sketch is shown in Fig. 15 where  $P_L$  is the cross-sectional length of the plate,  $L$  and  $B$  are the length and width of the tank, respectively. Fig. 16(a) presents

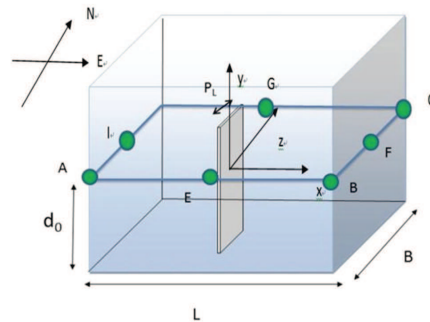


Figure 15: The definition sketch of a 3D tank with a vertical plate in the middle of tank.

the comparison between the present numerical results and the experimental data reported by Warnitchai & Pinkaew [16] and the results from asymptotic formula [15] and the agreement is very good. The further investigation of liquid sloshing in this type of plated tank under a resonant surge excitation is then discussed. The elevations of points A ( $H_A$ ) and C ( $H_C$ ) for a tank with a vertical plate excited at a frequency of  $1.0\omega_1$  are depicted in Fig. 16(b). In the analysis of sloshing liquid in a 3D tank under a resonant excitation without internal structures, the sloshing displacement at point A will continuously increase to a peak value. In the present simulation, the sloshing displacements of points A and C increase with time but reach peak at  $t = 5.5s$ . The resonant sloshing amplitude depicted in Fig. 16(b) is obviously reduced by the plate and the wave histories of points A and C become a little irregular after  $t = 5s$  because the free surface has been disturbed by the effect of the plate. The instantaneous snapshots of the free surface are illustrated in Fig. 17. It is obviously seen that two 3D holes appear near the edges of the plate and those holes are made by 3D vortices generated in the vicinity of the plate corners.

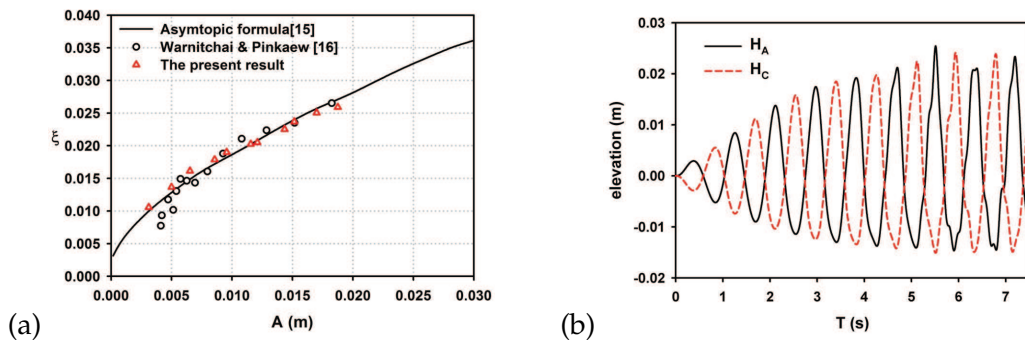


Figure 16: (a) The comparison between the present numerical results and the theoretical first-mode damping ratio  $\chi$  for the TLD with vertical plate tested by Warnitchai and Pinkaew as a function of wave amplitude. The effect of the energy dissipation at tank walls and bottom is included. (b) The wave histories at points A and C for a tank excited at a frequency of  $1.0\omega_1$  under surge motion.  $B/L=0.5$ ,  $P_L/B=0.25$ ,  $d_0/L=0.3$ ,  $x_0=0.005L$ .

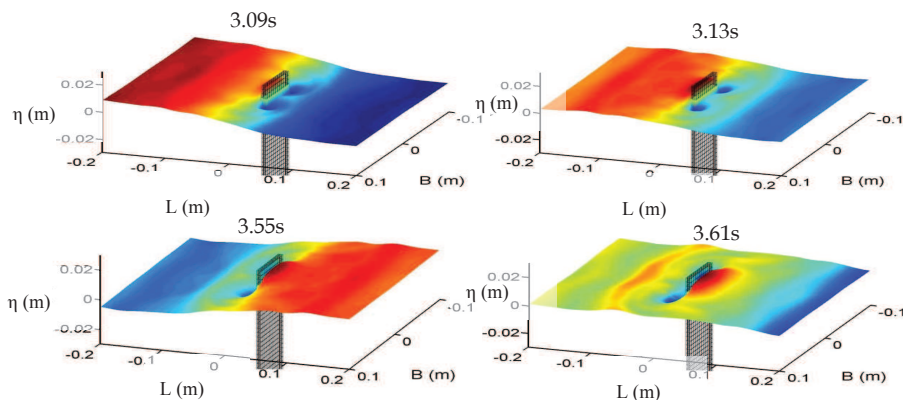


Figure 17: The snapshots of free surface for a tank with a vertical plate. The plated tank is the same as that in Fig. 16.

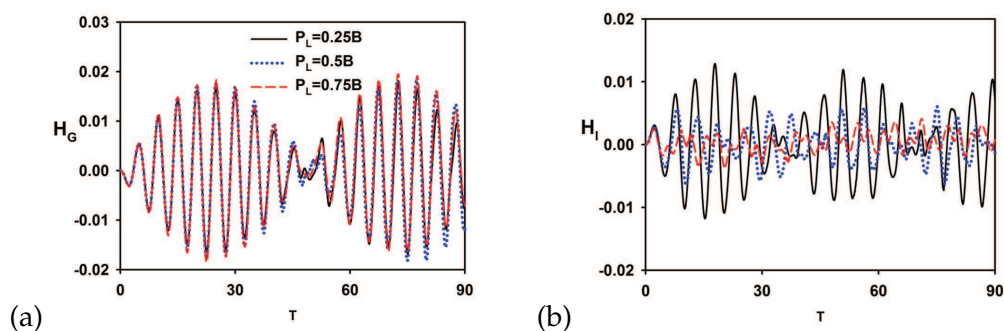


Figure 18: The comparisons of wave histories at points  $G$  and  $I$  for a tank with various lengths of vertical plate ( $P_L$ ) under diagonal forcing.  $H = \eta/d_0$  is the dimensionless wave elevation and  $T = t\sqrt{g/d_0}$  is the dimensionless time.  $d_0/L = 0.5$ ,  $a_0/L = 0.001$ ,  $\omega_x = \omega_z = 1.1\omega_1$ .

Wu and Chen [13] and Chen and Wu [14] reported in detail the classification and the characteristics of various sloshing waves for a tank excited at coupled surge-sway and surge-sway-heave motion without internal structures. In a tank under diagonal excitation, the diagonal waves are generated in the tank. In this study, the effect of the length ( $P_L$ ) of a vertical plate on the diagonal waves is demonstrated and discussed.

We mark the location of the absolute peak of the free surface at every instant of the sloshing. The wave histories of points  $G$  and  $I$ , the wave pattern, the distribution of wave peaks and the spectral analyses of  $H_G$  and  $H_I$  for a square base tank with  $d_0/L = 0.5$  and  $P_L/B = 0.25, 0.5$  and  $0.75$  under a diagonal forcing are illustrated in Figs. 18, 19, and 20, respectively. The different beating phenomena of  $H_G$  and  $H_I$  are presented in Fig. 18. The feature of the swirling waves is the peaks distribute along the tank walls and is demonstrated in Fig. 19(a). The peaks' distribution show in Fig. 19(b) presents the characteristic of the swirling-like waves. The diagonal wave type in a tank without internal structures is transferred to the swirling type due to the influence of the plate.

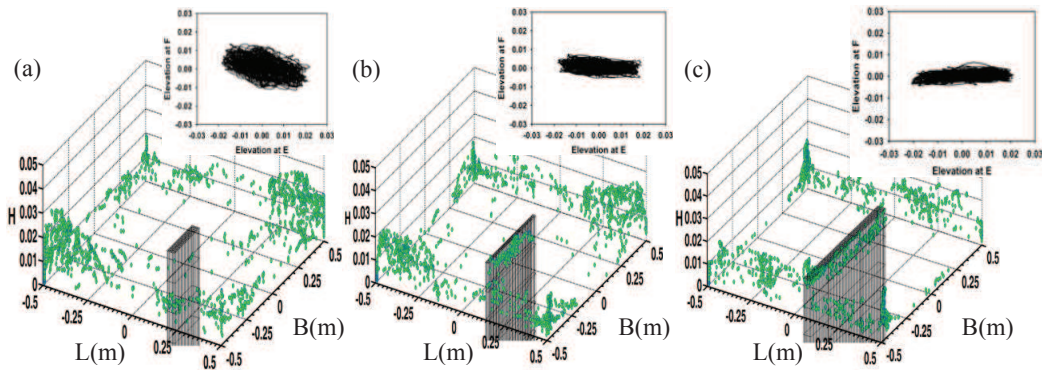


Figure 19: A 3D tank with a vertical plate under a diagonal excitation, the distribution of peaks (subplots: the wave pattern). (a)  $P_L/B=0.25$ ; (b)  $P_L/B=0.5$ ; (c)  $P_L/B=0.75$ .

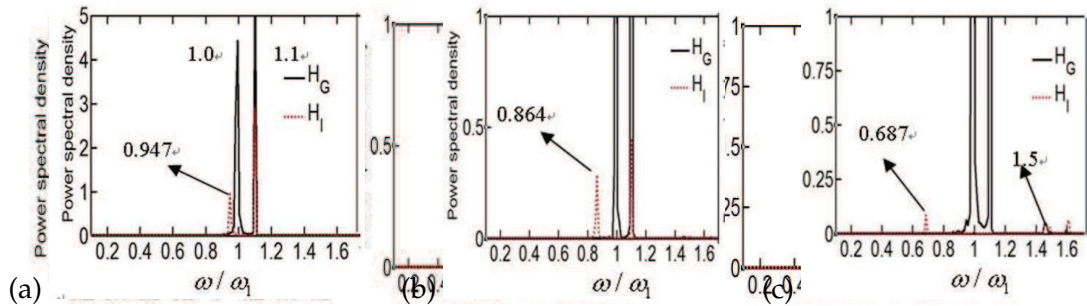


Figure 20: A 3D tank with a vertical plate under a diagonal excitation, the spectral analyses of  $H_G$  and  $H_I$ . (a)  $P_L/B=0.25$ ; (b)  $P_L/B=0.5$ ; (c)  $P_L/B=0.75$ ;  $d_0/L=0.5$ .

For  $P_L/B = 0.25$ , the distribution of absolute peak mostly concentrates in the vicinity of corners  $A$  and  $C$  of the tank. The spectral analysis of  $H_G$  shown in Fig. 20(a) reveals several peaks. The maximum one is contributed by the external forcing ( $1.1\omega_1$ ) and the second one ( $1.0\omega_1$ ) is the first natural frequency of the tank without internal structures. In addition to the mode of external forcing ( $1.1\omega_1$ ), the peak of  $0.947\omega_1$  is also demonstrated in the spectral analysis of  $H_I$ . The natural modes of a 3D square tank can be expressed as

$$\lambda_{i,j} = \pi \sqrt{i^2 + j^2}, \quad \omega_{i,j}^2 = g \lambda_{i,j} \tanh(\lambda_{i,j} d_0), \quad (4.2)$$

where  $i, j$  are the natural mode's components of  $x$ - and  $z$ -axes, respectively,  $g$  is the gravitational acceleration,  $d_0$  is still fluid depth and  $\omega_{i,j}$  are the natural frequencies of the 3-D tank. The wave modes in a 3D square tank, therefore, are composed by the contribution of  $i$  and  $j$  modes in the  $x$ - and  $z$ - axes, respectively. The plate in a tank would influence the shift of the resonant modes of the sloshing waves, particularly in the surge direction. As a result, the modes,  $0.947\omega_1$  and  $1.0\omega_1$ , can be correlated with the first natural modes in the  $x$  and  $z$  axes, respectively. Besides, it can be expected that as the length of the plate

increases, the reduction of the first natural mode of the waves in the  $x$  direction increases as well.

When the length of the plate increases to  $P_L/B = 0.5$ , the beating of  $H_I$  depicted in Fig. 18(b) is quite dissimilar to that of  $P_L/B = 0.25$ , and the swirling of waves is not as strong as that in the plated tank of  $P_L/B = 0.25$ . Further, the absolute peaks of the waves (Fig. 19(b)) predominantly distribute along the south and the north walls of the tank and some of them scatter along the wall of the plate. This indicates the waves mainly travel in the sway direction and this phenomenon also can be further discussed by the result shown in Fig. 20(b). There are three visible peaks appear in the spectral analyses of  $H_G$  and  $H_I$  (see Fig. 20(b)). The peak of  $0.864\omega_1$  can be correlated as the first natural mode in the  $x$  axis and the shift of the lowest natural mode in the  $x$  axis becomes obvious as the plate length increases. For a tank with a further longer plate ( $P_L/B = 0.75$ ), the wave elevations of points  $G$  and  $I$  (Fig. 18(c)) and the relationship of elevations between points  $E$  and  $F$  (Fig. 19(c)) demonstrates the dominant elevation is at points  $E$  and  $G$ . For the distribution of the peaks depicted in Fig. 19(c), the wave peaks mainly scatter on the north and south walls of the tank and along the plate and the characteristics of the swirling waves is not present anymore. In other words, the sloshing waves mainly travel in the transversal direction. Besides, the wave type of this case is dissimilar to those wave types that were discovered by Wu and Chen [19]. The influence of a longer plate results in the smaller gaps between the plate and the south or north tank wall. The original diagonal flow in a tank without internal structure becomes a sway-like wave. The dominant modes of the sloshing waves (see Fig. 20(c) as an example) are the external excitation frequency ( $1.1\omega_1$ ) and the first mode ( $1.0\omega_1$ ) of the wave in the  $z$  (sway) direction. The other two smaller modes,  $0.687\omega_1$  and  $1.5\omega_1$  are related to the first natural frequency in the  $x$  direction and the higher resonant mode of the waves, respectively.

## 5 Conclusions

A numerical scheme is developed and successfully used to study liquid sloshing in 2D and 3D tanks with internal structures. The numerical results were rigorously verified and extensive examples are made. The experiment setup with respect to the liquid sloshing in an unbaffled or baffled tank under coupled surge-sway motion was explored and a good agreement was presented between the experimental measurement and the computational results. The influence of a vertical plate in a 3D tank on the diagonal sloshing waves is investigated in detail. The following key conclusions are made: 1. The fictitious cell approach associated with a coordinate transformation technique is successfully used to solve for the sloshing fluid in 2D and 3D tanks with internal structures. 2. The stretch technique of grid system implemented in the present study assures the finer meshes around the tip of the baffles and the numerical simulation in this work can, therefore, capture the detailed local phenomenon of flow movement around the tip. 3. The effect of baffle height ( $d_b$ ) on the lowest natural frequency of the liquid tank is studied.

As the ratio  $d_b/d_0$  is large, the asymptotic formula [15] is inadequate to correctly predict the influence of internal baffles on the natural frequency of the tank. Based on the assumption of the potential flow theory [28], the boundary element method cannot describe the phenomenon of flow separation that would cause energy dissipation to affect the natural frequency of sloshing waves in tanks. The present results, therefore, might be more acceptable in predicting the natural frequency of a tank with bottom-mounted baffles. 4. The diagonal waves are transferred to the swirling waves because of the influence of the vertical plate. The length of the plate ( $P_L$ ) can cause a significant influence on not only the reduction of the lowest natural frequency of a partially fluid-filled tank but the type of the sloshing waves. 5. For a longer plate ( $P_L/B=0.75$ ), the original diagonal flow is conducted to a sway-like moving flow due to the smaller gaps between the plate and the south or north tank wall. 6. The design of the vertical plate mounted parallel to the east (west) wall of the tank is an effective tool to dampen the sloshing displacement in the surge direction. 7. The developed numerical scheme can be used to analyse sloshing liquid in 3D tanks with internal structures under six-degrees of freedom.

## Acknowledgments

Part of the paper has been presented in the 20th DSFD conference held at Fargo, ND, USA on Aug. 8 to 12, 2011. The study is partially supported by National Science Council under a grant NSC 99-2221-E-110-088 and a grant from Asia-Pacific research centre of NSYSU.

## References

- [1] H. N. Abramson, The dynamics of liquids in moving containers, NASA Rep, (1966), SP 106.
- [2] O. M. Faltinsen, O. F. Rognebakke and A. N. Timokha, Resonance three-dimensional nonlinear sloshing in a square-base basin, *J. Fluid Mech.*, 487 (2003), 1–42.
- [3] O. M. Faltinsen, O. F. Rognebakke and A. N. Timokha, Classification of three-dimensional nonlinear sloshing in a square-base tank with finite depth, *J. Fluids Structures.*, 20 (2005), 81–103.
- [4] O. M. Faltinsen, O. F. Rognebakke and A. N. Timokha, Resonant three-dimensional nonlinear sloshing in a square-base basin: part 2. effect of higher modes, *J. Fluid Mech.*, 523 (2005), 199–218.
- [5] B. F. Chen and S. W. Chiang, Complete 2D and fully nonlinear analysis of sloshing fluid in a rigid tank, *J. Eng. Mech.*, 125(1) (1999), 70–78.
- [6] P. C. Sames, D. Marcouly and T. Schellin, Sloshing in rectangular and cylindrical tank, *J. Ship Res.*, 46 (2002), 186–200.
- [7] J. B. Frandsen, Sloshing motions in excited tanks, *J. Comput. Phys.*, 196 (2004), 53–87.
- [8] B. F. Chen, Viscous fluid in tank under coupled surge, heave and pitch motions, *J. Waterway, Port Coastal Ocean Eng.*, 131(5) (2005), 239–256.
- [9] B. F. Chen and R. Nokes, Time-independent finite difference analysis of fully non-linear and viscous fluid sloshing in a rectangular tank, *J. Comput. Phys.*, 209 (2005), 47–81.

- [10] H. Akyildiz and N. E. Ünal, Experimental investigation of pressure distribution on a rectangular tank due to the liquid sloshing, *Ocean Eng.*, 32 (2005), 1503–1516.
- [11] H. Akyildiz and N. E. Ünal, Sloshing in a three-dimensional rectangular tank: numerical simulation and experimental validation, *Ocean Eng.*, 33 (2006), 2135–2149.
- [12] D. Liu and P. Lin, A numerical study of three-dimensional liquid sloshing in tanks, *J. Comput. Phys.*, 227 (2008), 3921–3939.
- [13] C. H. Wu and B. F. Chen, Sloshing waves and resonance modes of fluid in a 3D tank by a time-independent finite difference method, *Ocean Eng.*, 36 (2009), 500–510.
- [14] B. F. Chen and C. H. Wu, Effects of excitation angle and coupled heave-surge-sway motion on fluid sloshing in a three-dimensional tank, *J. Mar. Sci. Tech.*, 16 (2011), 22–50.
- [15] O. M. Faltinsen and A. N. Timokha, *Sloshing*, Cambridge University Press, 2009.
- [16] P. Warnitchai and T. Pinkaew, Modelling of liquid sloshing in rectangular tanks with flow-damping devices, *Eng. Struct.*, 20 (1998), 593–600.
- [17] M. Isaacson and S. Premasiri, Hydrodynamic damping due to baffles in a rectangular tank, *Can. J. Civ. Eng.*, 28 (2001), 608–616.
- [18] K. C. Biswal, S. K. Bhattacharyya and P. K. Sinha, Non-linear sloshing in partially liquid filled containers with baffles, *Int. J. Numer. Meth. Eng.*, 68 (2006), 317–337.
- [19] R. D. Firouz-Abadi, H. Haddadpour, M. A. Noorian and M. Ghasemi, A 3D BEM model for liquid sloshing in baffled tanks, *Int. J. Numer. Meth. Eng.*, 76 (2008), 1419–1433.
- [20] Y. Kim, Numerical simulation of sloshing flows with impact loads, *Appl. Ocean Res.*, 23 (2001), 53–62.
- [21] Y. Kim, Y. S. Shin and K. H. Lee, Numerical study on sloshing-induced impact pressures on three-dimensional prismatic tanks, *Appl. Ocean Res.*, 26 (2004), 213–226.
- [22] D. Liu and P. Lin, Three-dimensional liquid sloshing in a tank with baffles, *Ocean Eng.*, 36(2) (2009), 202–212.
- [23] P. K. Panigrahy, U. K. Saha and D. Maity, Experimental studies on sloshing behavior due to horizontal movement of liquids in baffled tanks, *Ocean Eng.*, 36 (2009), 213–222.
- [24] P. A. Berthelsen and O. M. Faltinsen, A local directional ghost cell approach for incompressible viscous flow problems with irregular boundaries, *J. Comput. Phys.*, 227 (2008), 4354–4397.
- [25] C. W. Hirt, B. D. Nicholas and N. C. Romero, SOLA-a numerical solution algorithm for transient fluid flows, Los Alamos Scientific Laboratory, Report LA-5852, 1975.
- [26] T. K. Hung and M. H. Wang, Nonlinear hydrodynamic pressure on rigid dams motion, *J. Eng. Mech. ASCE*, 113(4) (1987), 482–499.
- [27] T. K. Hung and B. F. Chen, Nonlinear hydrodynamic pressure on dams during earthquake, *J. Eng. Mech., ASCE* 116(6) (1990), 1372–1391.
- [28] O. M. Faltinsen, O. F. Rognebakke and A. N. Timokha, Resonant three-dimensional non-linear sloshing in a square-base basin: part 3. base ratio perturbations, *J. Fluid Mech.*, 551 (2006), 93–116.
- [29] O. M. Faltinsen, A numerical non-linear method of sloshing in tanks with two dimensional flow, *J. Ship Res.*, 22(3) (1978), 193–202.